Am J Nucl Med Mol Imaging 2024;14(1):31-40
www.ajnmmi.us /ISSN:2160-8407/ajnmmi0155049

Original Article

Noninvasive PET imaging of tumor PD-L1 expression with ^{64}Cu-labeled Durvalumab

Sara Malih[1], Wilson Lin[2], Zhongmin Tang[3], Molly C DeLuca[2], Jonathan W Engle[2], Behrouz Alirezapour[4], Weibo Cai[2,3], Mohammad J Rasaee[1]

[1]Department of Medical Biotechnology, Faculty of Medical Sciences, Tarbiat Modares University, Tehran, Iran; [2]Department of Medical Physics, University of Wisconsin-Madison, Madison, WI, USA; [3]Department of Radiology, University of Wisconsin-Madison, Madison, WI, USA; [4]Radiation Application Research School, Nuclear Science and Technology Research Institute (NSTRI), Tehran, Iran

Received December 20, 2023; Accepted February 4, 2024; Epub February 20, 2024; Published February 28, 2024

Abstract: Breast cancer (BrCa) ranks as the most prevalent malignant neoplasm affecting women worldwide. The expression of programmed death-ligand 1 (PD-L1) in BrCa has recently emerged as a biomarker for immunotherapy response, but traditional immunohistochemistry (IHC)-based methods are hindered by spatial and temporal heterogeneity. Noninvasive and quantitative PD-L1 imaging using appropriate radiotracers can serve to determine PD-L1 expression in tumors. This study aims to demonstrate the viability of PET imaging with ^{64}Cu-labeled Durvalumab (abbreviated as Durva) to assess PD-L1 expression using a murine xenograft model of breast cancer. Durvalumab, a human IgG1 monoclonal antibody against PD-L1, was assessed for specificity *in vitro* in two cancer cell lines (MDA-MB-231 triple-negative breast cancer cell line and AsPC-1 pancreatic cancer cell line) with positive and negative PD-L1 expression by flow cytometry. Next, we performed the *in vivo* evaluation of ^{64}Cu-NOTA-Durva in murine models of human breast cancer by PET imaging and *ex vivo* biodistribution. Additionally, mice bearing AsPC-1 tumors were employed as a negative control. Tumor uptake was quantified based on a 3D region-of-interest (ROI) analysis of the PET images and *ex vivo biodistribution* measurements, and the results were compared against conventional IHC testing. The radiotracer uptake was evident in MDA-MB-231 tumors and showed minimal nonspecific binding, corroborating IHC-derived results. The results of the biodistribution showed that the MDA-MB-231 tumor uptake of ^{64}Cu-NOTA-Durva was much higher than ^{64}Cu-NOTA-IgG (a nonspecific radiolabeled IgG). In Conclusion, ^{64}Cu-labeled Durvalumab PET/CT imaging offers a promising, noninvasive approach to evaluate tumor PD-L1 expression.

Keywords: Positron emission tomography (PET), programmed death-ligand 1 (PD-L1), breast cancer (BrCa), Durvalumab, ^{64}Cu, immunoPET

Introduction

Breast cancer (BrCa) is the most commonly diagnosed cancer among women worldwide and the leading cause of cancer-related deaths in women [1, 2]. The current standard-of-care treatments for BrCa are insufficient, as inherent or drug-induced resistance often underlies metastasis, relapse, and mortality [3, 4]. Programmed cell death ligand-1 (PD-L1) is an essential immune checkpoint that is ubiquitously expressed across a spectrum of malignant tumors and involved in the immune evasion process [5]. Immune checkpoint blockade therapy, which targets the programmed death protein 1 (PD-1) and its ligand PD-L1, has shown promising efficacy in treating BrCa and other malignancies [6, 7]. However, not all patients respond to this therapy, and there is a need for developing biomarkers to guide patient selection, predict response, and assist with combinatorial therapy [8, 9].

PD-L1 expression in tumor cells and tumor-associated immune cells are the most commonly investigated biomarker for immunotherapy, and several companion diagnostic tests for PD-L1 expression, including 22C3 and SP142 assays have been approved by the FDA [10, 11]. However, biopsy-based immunohistochemical (IHC) testing is limited by intra-tumoral and inter-lesional heterogeneity, which may lead to a lack of focal PD-L1 expression, dynamic changes in PD-L1 expression after therapeutic intervention, and poor uniformity in the determination of PD-L1 levels by different tests [12, 13]. Moreover, the localization of PD-L1 is challenging due to its presence on the surface and in the cytoplasm of tumor cells and immune cells [14, 15]. Conventional IHC assays often lack accuracy and reliability due to the interference caused by the staining of cytoplasmic proteins, which hampers accurate measurement of proteins on the cell membrane [16].

This dual localization impacts the detection and quantification of PD-L1, as surface PD-L1 plays a pivotal role in immune response modulation, while cytoplasmic PD-L1 may be involved in different intracellular processes. Accurately identifying and quantifying PD-L1 in these distinct cellular locations is crucial for understanding its role in tumor biology and for the effective application of targeted therapies [17, 18].

In contrast, *in vivo* techniques to assess PD-L1 expression via molecular imaging can be used to monitor disease progression, localize metastatic sites, and generate personalized therapies [19-23]. PET imaging with a positron-emitting radionuclide is a popular choice due to its high sensitivity, superb tissue penetration, reproducible quantification, and potential for clinical translation, among others [24-30]. U.S. Food and Drug Administration (FDA) has approved three anti-PD-L1 antibodies for the treatment of various types of cancer: Atezolizumab (Tecentriq), Durvalumab (Imfinzi), and Avelumab (Bavencio) [31]. Several immunoPET tracers targeting PD-L1 have been reported in pre-clinical and clinical studies [32-34]. Of these, Atezolizumab (Atz, MPDL3280A) is a practical option given its clinical usage and reliability in assessing PD-L1 expression in BrCa [35-37] and when labeled with zirconium-89 (^{89}Zr), it has been used in PET imaging to visualize PD-L1 expression in tumors. This tracer is beneficial due to the long half-life of ^{89}Zr, allowing for delayed imaging which matches the pharmacokinetics of antibodies. However, the long half-life may also increase the radiation dose to the patient [38, 39].

Similar to Atezolizumab, Durvalumab is another anti-PD-L1 antibody. Durvalumab, a fully human IgG1 monoclonal antibody targeting PD-L1, has a high affinity for PD-L1. Early human studies employing Durvalumab labeled with ^{89}Zr for evaluation of PD-L1 expression in squamous cell carcinoma of head and neck and non-small cell lung cancer (NSLC) patients have yielded promising results [40-42]. ^{124}I-labeled F(ab')$_2$ fragments of Durvalumab and ^{124}I-labeled Durvalumab have been used for PD-L1 expression in human NSLC tumors *in vivo*, as well [43]. FDA has approved Durvalumab for the treatment of urothelial carcinoma and other malignancies, and it is currently under phase I and II clinical trials for the combination therapy of BrCa [44-46]. These advancements have enhanced our confidence in the safety and feasibility of immunoPET imaging based on the tracer derived from Durvalumab. Furthermore, recent studies have used different radiotracers such as ^{89}Zr-Atezolizumab and ^{89}Zr-labeled Avelumab for assessing the PD-L1 expression using immune-PET imaging [47-49]. ^{89}Zr, with a half-life of about 78.4 hours, offers a longer imaging window, which can be beneficial for slower pharmacokinetics of antibodies but increases radiation exposure [50]. ^{64}Cu has a half-life of about 12.7 hours, which can be a good balance between providing enough time for the antibody to localize to the tumor and limiting radiation exposure [51]. Previous studies have demonstrated the feasibility of antibody labeling with ^{64}Cu [52] and its successful application in detecting PD-L1 expression patterns using PET/CT [32]. The *in vivo* findings indicated that ^{64}Cu-Atezolizumab has the specificity for detecting different levels of PD-L1 expression in Triple Negative Breast Cancers (TNBCs) using PET/CT, validating its use in varied PD-L1 detection [35].

In this study, we evaluated the efficacy of immunoPET for noninvasive monitoring of PD-L1 expression in BrCa using ^{64}Cu-NOTA-Durva. We confirmed the high expression of PD-L1 in MDA-MB-231 human BrCa cell line in murine xenograft models via biopsy IHC and validated the efficacy of this tracer for PET imaging. In our control experiments, we utilized the PD-L1 negative AsPC-1 tumor cell line with the ^{64}Cu-NOTA-Durva, and the PD-L1 positive MDA-MB-231 tumor cell line with the ^{64}Cu-NOTA-Rituximab, a nonspecific radiolabeled IgG.

Our results provide insights into the potential of immunoPET imaging with ^{64}Cu-NOTA-Durva as a noninvasive approach for monitoring of PD-L1 expression in BrCa.

Materials and methods

Chemicals

Durvalumab (anti-PD-L1) was obtained from Selleck Chemicals, Inc. (Houston, TX). 1,4,7-triazacyclononane-1,4,7-triacetic acid (p-SCN-Bn-NOTA) was purchased from Macrocyclics, Inc. (Dallas, TX). $^{64}CuCl_2$ in 0.05 M HCl was obtained from UW-Madison's cyclotron research group. PD-L1 (E1L3N) XP Rabbit monoclonal antibody was purchased from Cell Signaling, Inc. (Danvers, MA). PE anti-human CD274 (B7-H1, PD-L1) antibody was purchased from BioLegend, Inc. (San Diego, CA). APC Conjugation Kit - Lightning-Link was purchased from Abcam, Inc. (Boston, MA).

Rituximab (monoclonal anti-CD20 antibody) was purchased from Selleck Chemicals, Inc. (Houston, TX). PD-10 desalting columns were supplied by GE Healthcare, Inc. (Piscataway, NJ). 4',6-diamidino2-phenylindole (DAPI) is the product of ThermoFisher, Inc. (Burlingame, CA). Dulbecco Modified Eagle Medium (DMEM) was obtained from Gibco, Inc. (Grand Island, NY). Fetal bovine serum (FBS) was provided by Gibco, Inc. (Grand Island, NY). All other reagents were from ThermoFisher, Inc.

Cell culture

Human BrCa cell line MDA-MB-231 and human pancreas cancer cell line AsPC-1 were provided by the American Type Culture Collection (ATCC; Manassas, VA). The cells were cultured in DMEM and RPMI-1640 medium, respectively, with high glucose, FBS (10%), and Penicillin/streptomycin (1%). The T75 flasks containing the cells were placed in a humidified constant thermoincubator at 37°C with CO_2 (5%). Cells were trypsinized and harvested for tumor inoculation and *in vitro* experiments after reaching ~70% confluence.

Subcutaneous xenograft model

Female athymic nude mice aged 4 to 7 weeks were purchased from Envigo (Cambridge Shire, UK). Approximately 5×10^6 MDA-MB-231 cells and 4×10^6 AsPC-1 cells, suspended in 150 μL of medium were implanted subcutaneously on the right shoulder of each mouse. The injected mixture can be adsorbed in 1-2 days. At ~5 weeks post-inoculation of MDA-MB-231 cells and 10 days post-inoculation of AsPC-1 cells, tumors with a diameter of ~10 mm were accepted for *in vivo* experiments. 12-h light-dark cycle was maintained, and food and water were continuously available. All experiments complied with current regulations of the Institutional Animal Care and Use Committee (IACUC) at the University of Wisconsin-Madison (UW-Madison).

Identification of PD-L1 expression

Immunofluorescent staining and confocal imaging were conducted to validate the expression of PD-L1 on the MDA-MB-231 and AsPC-1 cell lines. The cells were cultured in glass-bottom dishes (50 mm, ~2×10^5 cells/dish) and incubated at 37°C in CO_2 (5%) overnight. Then cells were incubated with PE-anti-PD-L1, APC-Durvalumab (10 μg/mL), and DAPI (5 μg/mL) at 4°C overnight in the dark and imaged on an A1R confocal microscope (Nikon, Inc.; Melville, NY).

PD-L1 expression on the tumor cell surface was verified in the MDA-MB-231 and AsPC-1 cell lines by flow cytometry. The cells were suspended in a staining buffer (4°C) and split into aliquots of 1×10^6 cells/tube. Then the cells were incubated with PE-anti-PD-L1, APC-Durvalumab (10 μg/mL) for 1 h on ice in darkness. Finally, all cells were re-suspended in 500 μL of staining buffer (4°C) and DAPI was added 10 min before the flow cytometry analysis on a 5-Laser LSR Fortessa cytometer (Becton-Dickinson, Inc.; San Jose, CA). Cell counts were recorded and analyzed using FlowJo (ver. X.0.9; Tree Star, Inc.; Ashland, OR) software.

Chelator conjugation and radiolabeling

p-SCN-Bn-NOTA was dissolved in 10 μL of dimethyl-sulfoxide (DMSO) and Durvalumab was conjugated to NOTA at a molar ratio of 1:5 at pH 8.4. The mixture was incubated at room temperature (RT) for 2 h with constant shaking and later purified by size-exclusion columns using metal-free phosphate buffer solution (PBS) as the mobile phase to remove unbound NOTA. Fractions containing NOTA-conjugated Durvalumab were collected, and the peak fraction of solute was confirmed on the NanoDrop One (ThermoFisher; Waltham, MA). For ^{64}Cu radiolabeling, Durvalumab/IgG was incubated with $^{64}CuCl_2$ (111 MBq/3 mCi) in 300 μL of sodium acetate buffer (0.1 mol/L, pH 5) for 60 min at 37°C with constant shaking. The reaction solution was purified by PD-10 (PBS as the eluent). Eluted ^{64}Cu-NOTA-Durvalumab (^{64}Cu-NOTA-Durva) fractions were combined and used for mouse studies.

Serum stability testing of ^{64}Cu-NOTA-Durvalumab

The *in vitro* serum stability of ^{64}Cu-NOTA-Durva was assessed using instant thin-layer chromatography. 100 μCi (3.7 MBq) of ^{64}Cu-NOTA-Durva was incubated in 200 μL of human serum at 37°C for 4, 24, and 48 h.

PET imaging and biodistribution studies

In vivo PET imaging was performed using an Inveon Micropet/CT scanner (Siemens Medical Solutions USA, Inc.). Tumor xenograft mice (n = 3/group) were injected with 3.7-7.4 MBq (0.10-0.20 mCi) of ^{64}Cu-NOTA-Durvalumab/NOTA-IgG via the lateral tail vein. PET/CT scans were acquired at 4, 24, and 48 h post-injection (p.i.). The Inveon Research Workplace (IRW) software (Siemens, Inc.) was used to quantify the mean uptake of the region of interest (ROI) in major organs in terms of the percentage of injected dose per gram (%ID/g, decay-corrected). The %ID/g value was calculated by dividing tissue activity in MBq/g (converted from ROI uptake) by the total radioactive dose injected.

Ex vivo biodistribution studies were carried out after the last PET scan at 48 h p.i. and all mice were euthanized by CO_2 asphyxiation. The tumor, blood, brain, heart, lung, liver, spleen, kidneys, stomach, intestine, muscle, bone, and pancreas were harvested and wet weighed. The radioactivity of major organs was determined using a Wizard 2480 automatic γ-counter (PerkinElmer, Inc.; Waltham, MA), and the results are presented as %ID/g, mean ± standard deviation.

Immunohistochemistry

Tumors were excised from mice, fixed overnight in 4% paraformaldehyde, and subsequently transferred to 70% ethanol for preservation. Immunohistochemical analysis was performed at the University of Wisconsin-Madison's Translational Research Initiatives in Pathology (TRIP) facility. The samples were embedded in paraffin for tissue processing. Deparaffinization was achieved using standard protocols, followed by heat-induced epitope retrieval using an EDTA-based buffer (Ventana #950-500) at 95°C for 32 minutes. The primary antibody (E1L3N®) XP® Rabbit mAb #13684 was applied at a dilution of 1:100 and incubated at 37°C for 32 minutes. The secondary antibody, Discovery OmniMap anti-Rabbit HRP (Ventana #760-4311), was applied and incubated at 37°C for 16 minutes. Counterstaining was performed with Harris hematoxylin at a 1:5 dilution for 30 seconds, and the slides were then covered with xylene. Finally, the slides were imaged using ImageScope.

Statistical analysis

Quantitative data were analyzed using GraphPad PRISM (version 10.1.1) and presented as mean ± standard deviation (SD).

Results

PD-L1 expression

As depicted in **Figure 1A**, the nuclei of MBA-MB-231 cells were stained by DAPI (blue channel). The PD-L1 on the cells was heavily stained by APC-Durvalumab and exhib-

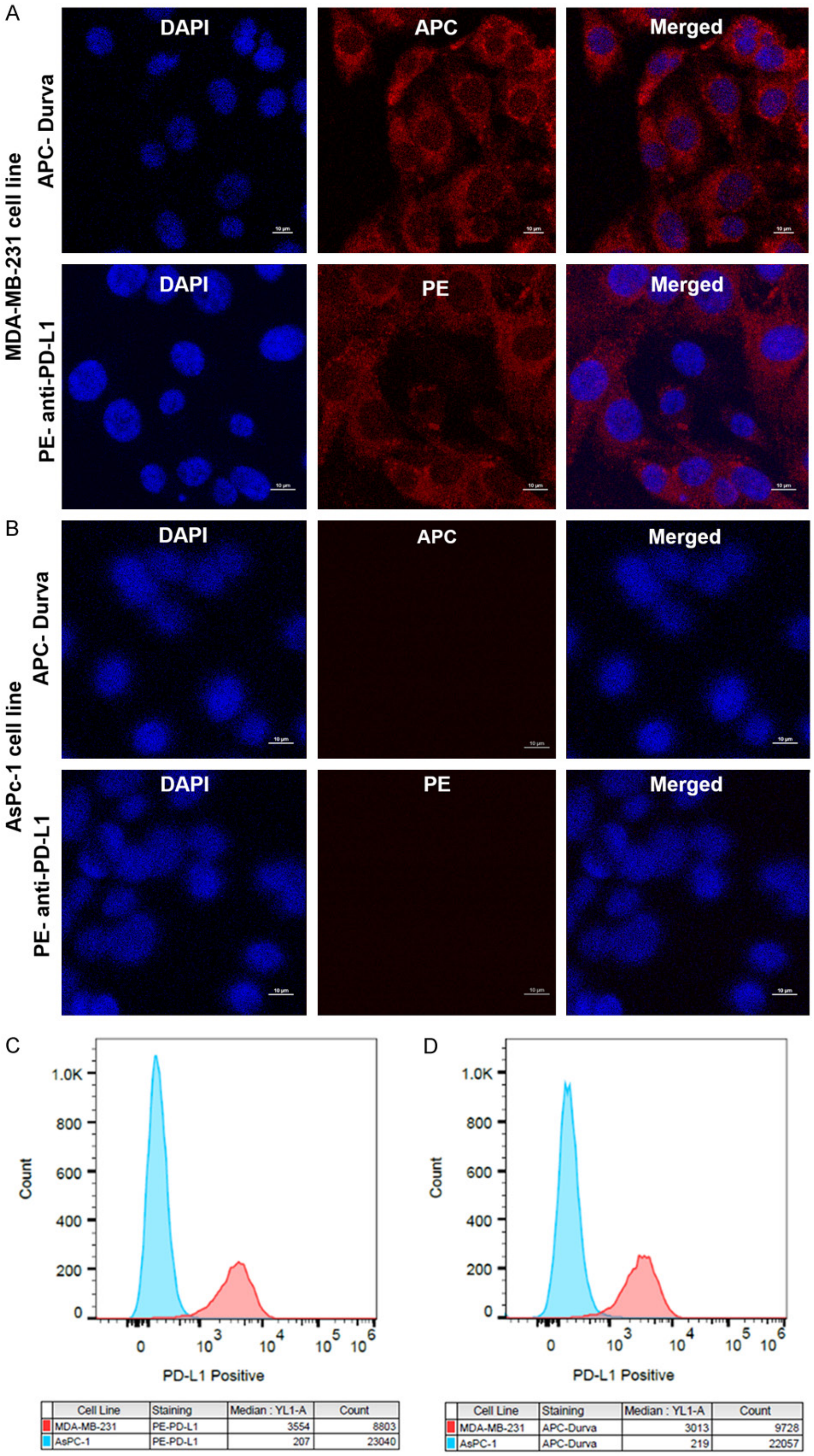

Figure 1. Characterization of *in vitro* PD-L1 expression in human BrCa cell line. A, B. The confocal imaging of MDA-MB-231 and AsPC-1 cells after immuno-fluorescent staining, Scale bar: 10 μm. A. MDA-MB-231 cells stained by APC-Durva and PE-anti-PD-L1. B. AsPC-1 cells stained by APC-Durva and PE-anti-PD-L1. Sample groups: DAPI, the nucleus stained by DAPI; APC, the PD-L1 expression stained by APC-Durvalumab; PE, the PD-L1 expression stained by PE-anti-PD-L1. C, D. The PD-L1 expression on the cell membrane of the MDA-MB-231 and AsPC-1 cell lines were evaluated using flow cytometry. C. The cell lines were stained by a commercialized PE-anti-PD-L1 antibody. D. The cell lines were stained by APC-Durva antibody. The blue area represents cells without PD-L1 expression, and the red area represents cells with PD-L1 expression. There is a significant shift in both Anti-PD-L1 antibody and Durvalumab treated group in MDA-MB-231 PD-L1 positive cell line compared to AsPC-1 PD-L1 negative cell line.

ited strong fluorescence (red channel), the cells engaging with PE-anti-PD-L1 antibody showed an intense red fluorescent signal as well. This verifies the high expression of PD-L1 on the MDA-MB-231 cell line. AsPC-1 PD-L1 negative cell lines (**Figure 1B**) were also stained to confirm the specificity of APC-Durvalumab binding. The nuclei of AsPC-1 cells were stained by DAPI (blue channel) and there was no significant PD-L1 expression on these cells after staining with APC-Durvalumab/PE-anti-PD-L1 antibody.

In the results of flow cytometry, cells stained with PE-anti-PD-L1 (**Figure 1C**) and APC-Durva (**Figure 1D**) shared notable positive shifts compared with control groups, confirming the high expression of PD-L1 on the MDA-MB-231 cell surface. The shift in the PD-L1 negative group of flow cytometry and the negative signal in the confocal images of the PD-L1 negative group is circumstantial evidence of the specificity APC-Durva. The *in vitro* results demonstrate that the MDA-MB-231 cell line is PD-L1 positive and Durvalumab shows specificity for PD-L1.

Radiochemistry

Durvalumab was successfully conjugated with NOTA and radiolabeled with ^{64}Cu. The ^{64}Cu-labeling achieved a radiochemical yield of >80% ^{64}Cu-NOTA-Durva. RTLC analysis results showed that ^{64}Cu-NOTA-Durva has high stability in serum, with >74% radiochemical purity at 48 h (**Figure 2**).

PET/CT imaging and biodistribution of ^{64}Cu-NOTA-Durvalumab

Figure 3 shows the PET/CT images and biodistribution results of ^{64}Cu-NOTA-Durva. ^{64}Cu-NOTA-Durva showed noticeable tumor uptake differences between the targeting and non-targeting groups at all timepoints from 4 to 48 h p.i. ^{64}Cu-NOTA-Durva showed longer blood retention in the non-targeting group. We further performed a biodistribution study at 48 h p.i.

Histology

Tumor samples were fixed in PFA 4% overnight and then transferred to cold Ethanol 70%. Slide scans of these tissues after

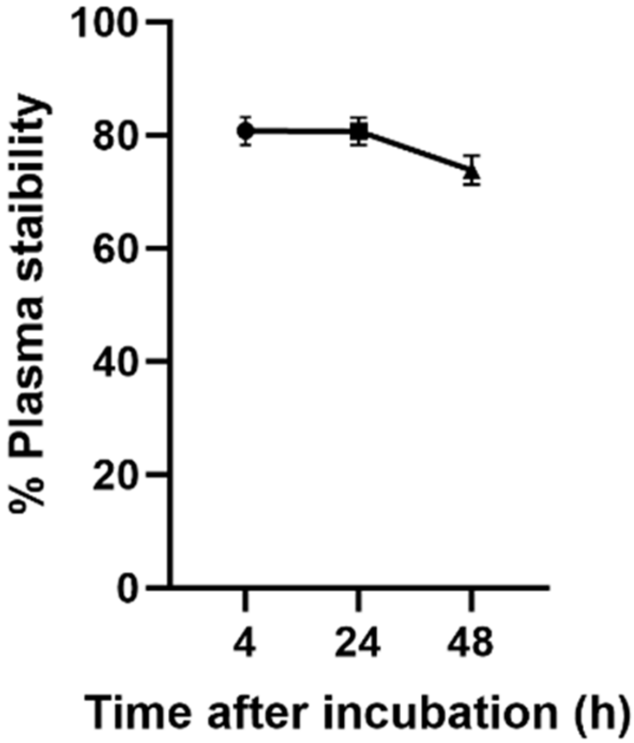

Figure 2. RTLC analysis of ^{64}Cu-NOTA-Durva. The radiochemical purity of ^{64}Cu-NOTA-Durva was ≥74% after 48 h incubation in serum. n = 3.

immunofluorescent staining are shown in **Figure 4**. The fluorescence from PD-L1 of MDA-MB-231 (in brown) is visible and overlays with the cell nuclei (in blue) in tumor tissue.

Discussion

The level of PD-L1 expression has been shown to greatly influence the patient's response to therapy [53, 54] and could be a superior predictor of patient response to immune checkpoint blockade compared to biopsy IHC analysis, which is the current clinical standard [10]. However, PD-L1 expression is not consistently stable on the cell surface and can be influenced by various signaling pathways, post-translational modifications, and the release of inflammatory factors during treatments like radiotherapy and chemotherapy [40-43, 55].

In light of these challenges, the development of advanced imaging techniques such as PD-L1 PET imaging becomes imperative. By allowing noninvasive and real-time monitoring of PD-L1 expression, PD-L1 PET imaging offers a valuable tool for accurately assessing PD-L1 status and guiding treatment decisions. This imaging modality overcomes the limitations of traditional methods and provides timely information on PD-L1 expression dynamics, ensuring optimal patient selection and treatment efficacy.

Several studies have investigated tumor detection using molecular imaging based on PD-L1 expression, often using murine models [32-37, 56, 57]. This study differs from previous ones in a few key aspects. Firstly, human cell lines were used to induce the tumor models, enhancing clinical translatability compared to studies using murine cell lines such as 4T1 [58-60]. Secondly, the positive cell line used in this study (MDA-MB-231) expresses native levels of PD-L1 without artificial overexpression, unlike some previous studies that have used human PD-L1 gene-transfected A375 cells and human PD-L1-gene transfected B16-F10 [61, 62]. Lastly, the study avoided predosing/blocking strategies employed in other studies [48, 61, 63] to minimize off-target lymphatic uptake. Only the radiolabeled protein was administered at a low dose to avoid potential pharmacologic responses while achieving sufficient imaging signal. Predosing involves administering an excess of unlabeled antibody before introducing the radiolabeled counterpart, aiming to saturate target binding sites in normal tissues, thus reducing background signal. Some studies have highlighted the advantages of predosing in improving image quality and target-to-background ratios, emphasizing its potential clinical relevance [64]. Predosing or blocking strategies, while effective in minimizing non-specific binding, can introduce complexities such as altering the pharmacokinetics of the radiotracer, potentially influencing its distribution and clearance patterns [48, 65, 66]. The choice to avoid these strategies in the current study aimed to maintain simplicity in the experimental design and enhance the reliability of the obtained imaging data.

PD-L1 imaging presents challenges compared to traditional tumor markers. The widespread expression of PD-L1 reduces the imaging signal in tumors, and conventional control experiments cannot be applied. As the injection of a blocking dose would saturate PD-L1 in the spleen and lymph nodes, this method might lead to increased tracer accumulation in the tumor, challenging its specificity for cancer cells, contrary to conventional studies. Using a nonspecific, isotype-matched antibody as a control also presents issues, as it would not bind to ubiquitous PD-L1 throughout the body and may accumulate to higher levels in tumor tissue that were elaborated in previous studies [47, 67]. In our study, as a negative control, mice with AsPC-1 tumors were used to assess the ^{64}Cu-NOTA-Durva accumulation in tumor tissues not attributed to PD-L1 expression by tumor cells. Furthermore, nonspecific uptake was assessed by a radiolabeled control IgG antibody, ^{64}Cu-NOTA-IgG, in MDA-MB-231 mice models.

The choice of PD-L1-targeted radiotracer for immunoPET imaging depends on the specific requirements of the study, including the desired imaging window, the balance between resolution and radiation dose, and the pharmacokinetic properties of the tracer in relation to the tumor characteristics. ^{64}Cu has a half-life of approximately 12.7 hours. Our study benefits from the relatively short half-life of the ^{64}Cu, enabling multiple imaging sessions in a day

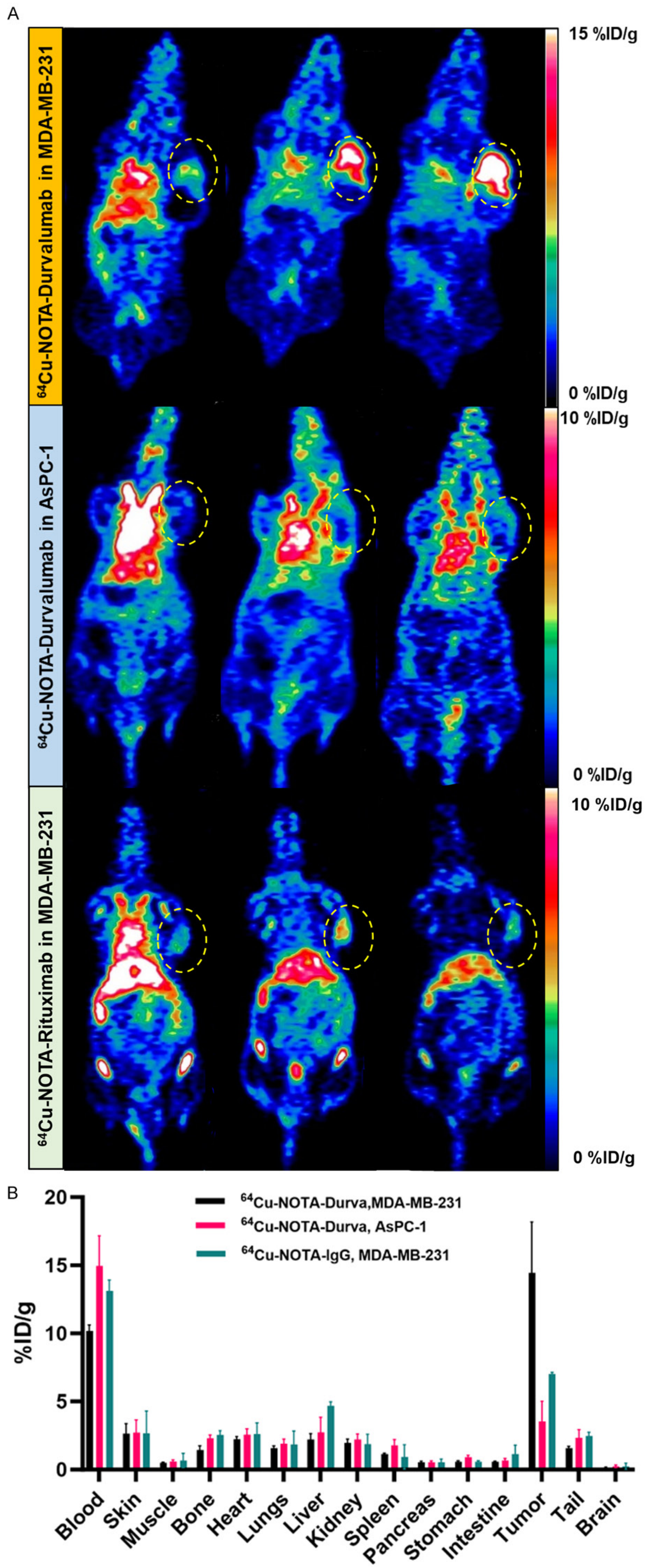

Figure 3. Representative PET/CT images and biodistribution of MDA-MB-231 and AsPC-1 tumor-bearing mice over time. Representative PET/CT images (A) and biodistribution (B) of MDA-MB-231 and AsPC-1 tumor-bearing mice injected with ^{64}Cu-NOTA-Durva/^{64}Cu-NOTA-IgG. n = 3.

and capturing changes in PD-L1 expression over shorter time spans. Furthermore, shorter-lived radionuclides like ^{64}Cu typically result in lower radiation exposure for patients and medical personnel, enhancing safety in clinical settings. ^{64}Cu is more accessible and easier to handle in many clinical settings, which can streamline the logistics of our study as well.

On the other hand, ^{89}Zr forms stable chelates with antibodies, ensuring long-lasting imaging signals. However, for our specific study, the shorter half-life of ^{64}Cu may still provide sufficient stability while offering more flexibility in imaging scheduling. In summary, based on the title and focus of our study on breast cancer and PD-L1 expression using ^{64}Cu-labeled Durvalumab, ^{64}Cu appears to be a suitable choice. Its shorter half-life, rapid imaging capabilities, and lower radiation exposure align well with the objectives of noninvasively evaluating PD-L1 expression dynamics in breast cancer tumors.

The results presented in this study demonstrate the successful conjugation of NOTA with Durvalumab and its radiolabeling with ^{64}Cu, resulting in a stable and pure ^{64}Cu-NOTA-Durva tracer. The *in vitro* experiments also showed high expression of PD-L1 on the MDA-MB-231 cell line, which indicates that Durvalumab can be a promising tracer for PD-L1 imaging in breast cancer.

The *in vivo* PET/CT imaging and biodistribution studies of ^{64}Cu-NOTA-Durva showed noticeable tumor uptake differences between the targeting and non-targeting groups, confirming the specificity of the tracer for PD-L1 positive tumors (14.47 ± 3.70 %ID/g for ^{64}Cu-NOTA-Durva vs 5.55 ± 2.5 %ID/g for ^{64}Cu-NOTA-IgG; n = 3). A five-fold higher uptake of radioactivity in MDA-M231 cells than in AsPC-1 cells further confirmed the specificity of ^{64}Cu-NOTA-Durva for PD-L1. The biodistribution study at 48 h p.i. further supported the selective accumulation of the tracer in the tumor, as evidenced by the higher uptake of the targeting group compared to the non-targeting group. The immunofluorescent staining of tumor tissue and flow cytometry results also confirmed the expression of PD-L1 in the MDA-MB-231 tumors. The findings of this

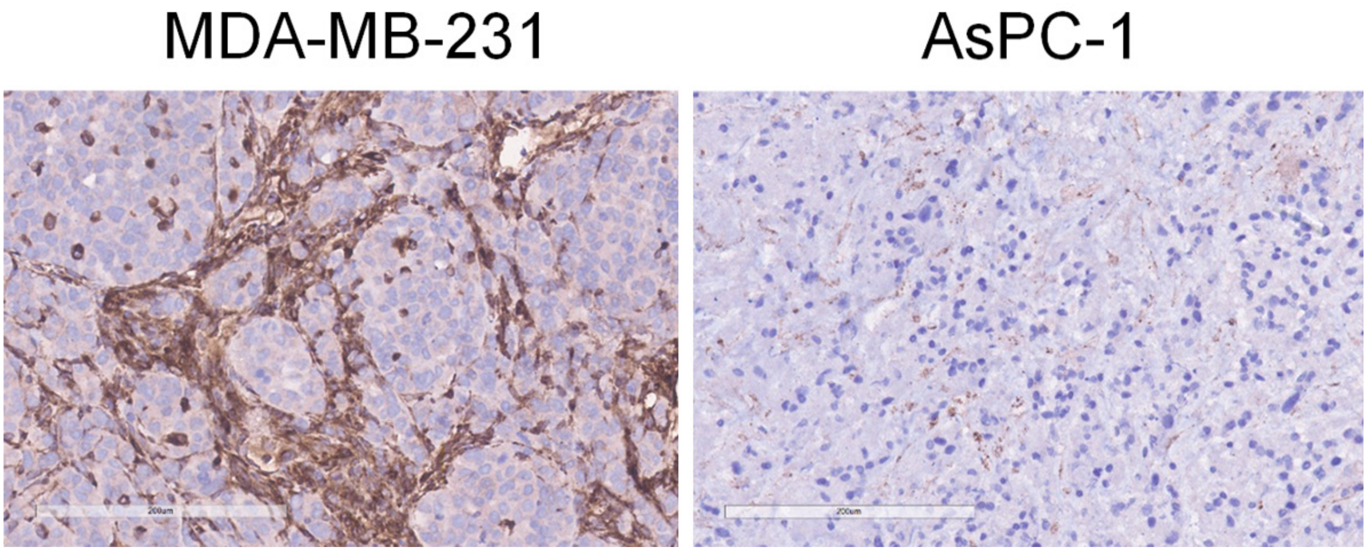

Figure 4. Assessment of PD-L1 expression pattern in MDA-MB-231 and AsPC-1 tumor samples using immunohistochemistry, Scale bar: 200 μm. Strong PD-L1 staining is observed in MDA-MB-231, indicating high expression levels, and very little staining in AsPC-1 tumor sample indicating low expression level.

study are consistent with previous studies that have used Durvalumab as a tracer for PD-L1 imaging in various types of cancer [42, 43].

Conclusion

Our study demonstrates the potential of PD-L1 PET/CT imaging with ^{64}Cu-labeled Durvalumab for noninvasive evaluation of PD-L1 expression in tumors. The radiolabeling of Durvalumab with ^{64}Cu was straightforward, and the radiolabeled compound showed high *in vitro* serum stability and specificity for PD-L1-expressing cells. The PET/CT imaging studies showed that ^{64}Cu-labeled Durvalumab can accumulate in PD-L1-expressing tumors and provide high-contrast images. The quantitative measurement of PD-L1 expression using PET/CT imaging with ^{64}Cu-labeled Durvalumab showed a significant correlation with PD-L1 expression levels in tumors, and the specificity of ^{64}Cu-labeled Durvalumab binding to PD-L1 was confirmed by non-targeting models. The results from this work can help guide the development of new PD-L1 inhibitors and improve our understanding of the role of PD-L1 in cancer biology.

Acknowledgements

This work was supported by the University of Wisconsin-Madison, the National Institutes of Health (P30 CA014520), and the Tarbiat Modares University.

Disclosure of conflict of interest

Weibo Cai declares conflict of interest with the following corporations: Actithera, Inc., Portrai, Inc., rTR Technovation Corporation, Four Health Global Pharmaceuticals Inc., and POP Biotechnologies, Inc.

Address correspondence to: Behrouz Alirezapour, Radiation Application Research School, Nuclear Science and Technology Research Institute (NSTRI), Tehran, Iran. E-mail: balirezapour@aeoi.org.ir; Weibo Cai, Department of Medical Physics, University of Wisconsin-Madison, Madison, WI, USA. E-mail: wcai@uwhealth.org; Mohammad J Rasaee, Department of Medical Biotechnology, Faculty of Medical Sciences, Tarbiat Modares University, Tehran, Iran. E-mail: rasaee_m@modares.ac.ir

References

[1] Siegel RL, Miller KD and Jemal A. Cancer statistics, 2020. CA Cancer J Clin 2020; 70: 7-30.
[2] Torre LA, Islami F, Siegel RL, Ward EM and Jemal A. Global cancer in women: burden and trends. Cancer Epidemiol Biomarkers Prev 2017; 26: 444-457.
[3] Holohan C, Van Schaeybroeck S, Longley DB and Johnston PG. Cancer drug resistance: an evolving paradigm. Nat Rev Cancer 2013; 13: 714-726.
[4] Ribatti D, Tamma R and Annese T. Epithelial-mesenchymal transition in cancer: a historical overview. Transl Oncol 2020; 13: 100773.
[5] Ghosh C, Luong G and Sun Y. A snapshot of the PD-1/PD-L1 pathway. J Cancer 2021; 12: 2735-2746.
[6] Schmid P, Adams S, Rugo HS, Schneeweiss A, Barrios CH, Iwata H, Diéras V, Hegg R, Im SA, Shaw Wright G, Henschel V, Molinero L, Chui SY, Funke R, Husain A, Winer EP, Loi S and Emens LA; IMpassion130 Trial Investigators. Atezolizumab and nab-paclitaxel in advanced triple-negative breast cancer. N Engl J Med 2018; 379: 2108-2121.
[7] Emens LA, Cruz C, Eder JP, Braiteh F, Chung C, Tolaney SM, Kuter I, Nanda R, Cassier PA, Delord JP, Gordon MS, ElGabry E, Chang CW, Sarkar I, Grossman W, O'Hear C, Fassò M, Molinero L and Schmid P. Long-term clinical outcomes and biomarker analyses of atezolizumab therapy for patients with metastatic triple-negative breast cancer: a phase 1 study. JAMA Oncol 2019; 5: 74-82.

[8] Disis ML and Stanton SE. Triple-negative breast cancer: immune modulation as the new treatment paradigm. Am Soc Clin Oncol Educ Book 2015; 2015: e25-e30.
[9] McGranahan N and Swanton C. Clonal heterogeneity and tumor evolution: past, present, and the future. Cell 2017; 168: 613-628.
[10] Carvajal-Hausdorf DE, Schalper KA, Neumeister VM and Rimm DL. Quantitative measurement of cancer tissue biomarkers in the lab and in the clinic. Lab Invest 2015; 95: 385-396.
[11] Hirsch FR, McElhinny A, Stanforth D, Ranger-Moore J, Jansson M, Kulangara K, Richardson W, Towne P, Hanks D, Vennapusa B, Mistry A, Kalamegham R, Averbuch S, Novotny J, Rubin E, Emancipator K, McCaffery I, Williams JA, Walker J, Longshore J, Tsao MS and Kerr KM. PD-L1 immunohistochemistry assays for lung cancer: results from phase 1 of the blueprint PD-L1 IHC assay comparison project. J Thorac Oncol 2017; 12: 208-222.
[12] Devarakonda S, Rotolo F, Tsao MS, Lanc I, Brambilla E, Masood A, Olaussen KA, Fulton R, Sakashita S, McLeer-Florin A, Ding K, Le Teuff G, Shepherd FA, Pignon JP, Graziano SL, Kratzke R, Soria JC, Seymour L, Govindan R and Michiels S. Tumor mutation burden as a biomarker in resected non-small-cell lung cancer. J Clin Oncol 2018; 36: 2995-3006.
[13] Scheel AH, Dietel M, Heukamp LC, Jöhrens K, Kirchner T, Reu S, Rüschoff J, Schildhaus HU, Schirmacher P, Tiemann M, Warth A, Weichert W, Fischer RN, Wolf J and Buettner R. Harmonized PD-L1 immunohistochemistry for pulmonary squamous-cell and adenocarcinomas. Mod Pathol 2016; 29: 1165-1172.
[14] McLaughlin J, Han G, Schalper KA, Carvajal-Hausdorf D, Pelekanou V, Rehman J, Velcheti V, Herbst R, LoRusso P and Rimm DL. Quantitative assessment of the heterogeneity of PD-L1 expression in non-small-cell lung cancer. JAMA Oncol 2016; 2: 46-54.
[15] Kleinovink JW, Marijt KA, Schoonderwoerd MJA, van Hall T, Ossendorp F and Fransen MF. PD-L1 expression on malignant cells is no prerequisite for checkpoint therapy. OncoImmunology 2017; 6: e1294299.
[16] Zhao X, Bao Y, Meng B, Xu Z, Li S, Wang X, Hou R, Ma W, Liu D, Zheng J and Shi M. From rough to precise: PD-L1 evaluation for predicting the efficacy of PD-1/PD-L1 blockades. Front Immunol 2022; 13: 920021.
[17] Wu Y, Chen W, Xu ZP and Gu W. PD-L1 distribution and perspective for cancer immunotherapy-blockade, knockdown, or inhibition. Front Immunol 2019; 10: 2022.
[18] Feng C, Zhang L, Chang X, Qin D and Zhang T. Regulation of post-translational modification of PD-L1 and advances in tumor immunotherapy. Front Immunol 2023; 14: 1230135.
[19] Michot JM, Bigenwald C, Champiat S, Collins M, Carbonnel F, Postel-Vinay S, Berdelou A, Varga A, Bahleda R, Hollebecque A, Massard C, Fuerea A, Ribrag V, Gazzah A, Armand JP, Amellal N, Angevin E, Noel N, Boutros C, Mateus C, Robert C, Soria JC, Marabelle A and Lambotte O. Immune-related adverse events with immune checkpoint blockade: a comprehensive review. Eur J Cancer 2016; 54: 139-148.
[20] Dhingra VK, Mahajan A and Basu S. Emerging clinical applications of PET based molecular imaging in oncology: the promising future potential for evolving personalized cancer care. Indian J Radiol Imaging 2015; 25: 332-341.
[21] Leung D, Bonacorsi S, Smith RA, Weber W and Hayes W. Molecular imaging and the PD-L1 pathway: from bench to clinic. Front Oncol 2021; 11: 698425.
[22] Medina-Ornelas S, García-Perez F, Estrada-Lobato E and Ochoa-Carrillo F. (68)Ga-PSMA PET/CT in the evaluation of locally advanced and metastatic breast cancer, a single center experience. Am J Nucl Med Mol Imaging 2020; 10: 135-142.
[23] Gelezhe PB, Blokhin IA, Marapov DI and Morozov SP. Quantitative parameters of MRI and (18)F-FDG PET/CT in the prediction of breast cancer prognosis and molecular type: an original study. Am J Nucl Med Mol Imaging 2020; 10: 279-292.
[24] Ayubcha C, Amanullah A, Patel KH, Teichner E, Gokhale S, Marquez-Valenzuela U, Werner TJ and Alavi A. Stroke and molecular imaging: a focus on FDG-PET. Am J Nucl Med Mol Imaging 2023; 13: 51-63.
[25] Hotsumi H, Ishii S, Suenaga H, Sugawara S, Fukushima K and Ito H. Investigation of tumor assessment between two PET systems using various indices: comparison between PET/CT and PET/MRI systems. Am J Nucl Med Mol Imaging 2023; 13: 156-163.
[26] Jiang H, Guo Y and Muzik O. Automated radiosynthesis of [(18)F]FMPEP-d(2) for cannabinoid receptor PET imaging. Am J Nucl Med Mol Imaging 2023; 13: 171-178.
[27] Li X, Li J, Zhou P, Li D, Wang M, Tong Q, Chen J, Zuo C, Zhang L and Li R. The functional views on response of host rabbit post coronavirus vaccination via ACE2 PET. Am J Nucl Med Mol Imaging 2023; 13: 43-50.
[28] Tan JL, Xia L, Sun SG, Zeng H, Lu DY and Cheng XJ. Prediction of EGFR mutation status in lung adenocarcinoma based on (18)F-FDG PET/CT radiomic features. Am J Nucl Med Mol Imaging 2023; 13: 230-244.
[29] Wilson ZJ, Xu G, Tewari SO and Lu Y. Comparison of PSMA-based (18)F-DCFPyL PET/CT and Tc-99m MDP bone scan in detection of bone metastasis in prostate cancer. Am J Nucl Med Mol Imaging 2023; 13: 1-10.
[30] Wu Y, Sun X, Zhang B, Zhang S, Wang X, Sun Z, Liu R, Zhang M and Hu K. Marriage of radiotracers and total-body PET/CT rapid imaging system: current status and clinical advances. Am J Nucl Med Mol Imaging 2023; 13: 195-207.
[31] Twomey JD and Zhang B. Cancer immunotherapy update: FDA-approved checkpoint inhibitors and companion diagnostics. AAPS J 2021; 23: 39.
[32] Hettich M, Braun F, Bartholomä MD, Schirmbeck R and Niedermann G. High-resolution PET imaging with therapeutic antibody-based PD-1/PD-L1 checkpoint tracers. Theranostics 2016; 6: 1629-40.
[33] Chatterjee S, Lesniak WG, Gabrielson M, Lisok A, Wharram B, Sysa-Shah P, Azad BB, Pomper MG and Nimmagadda S. A humanized antibody for imaging immune checkpoint ligand PD-L1 expression in tumors. Oncotarget 2016; 7: 10215-10227.
[34] Donnelly DJ, Smith RA, Morin P, Lipovšek D, Gokemeijer J, Cohen D, Lafont V, Tran T, Cole EL, Wright M, Kim J, Pena A, Kukral D, Dischino DD, Chow P, Gan J, Adelakun O, Wang XT, Cao K, Leung D, Bonacorsi SJ Jr and Hayes W. Synthesis and biologic evaluation of a novel 18F-Labeled adnectin as a PET radioligand for imaging PD-L1 expression. J Nucl Med 2018; 59: 529-535.
[35] Lesniak WG, Chatterjee S, Gabrielson M, Lisok A, Wharram B, Pomper MG and Nimmagadda S. PD-L1 detection in tu-

mors using [(64)Cu]atezolizumab with PET. Bioconjug Chem 2016; 27: 2103-2110.

[36] Herbst RS, Soria JC, Kowanetz M, Fine GD, Hamid O, Gordon MS, Sosman JA, McDermott DF, Powderly JD, Gettinger SN, Kohrt HE, Horn L, Lawrence DP, Rost S, Leabman M, Xiao Y, Mokatrin A, Koeppen H, Hegde PS, Mellman I, Chen DS and Hodi FS. Predictive correlates of response to the anti-PD-L1 antibody MPDL3280A in cancer patients. Nature 2014; 515: 563-567.

[37] Fehrenbacher L, Spira A, Ballinger M, Kowanetz M, Vansteenkiste J, Mazieres J, Park K, Smith D, Artal-Cortes A, Lewanski C, Braiteh F, Waterkamp D, He P, Zou W, Chen DS, Yi J, Sandler A and Rittmeyer A; POPLAR Study Group. Atezolizumab versus docetaxel for patients with previously treated non-small-cell lung cancer (POPLAR): a multicentre, open-label, phase 2 randomised controlled trial. Lancet 2016; 387: 1837-1846.

[38] Bridgwater C, Geller A, Hu X, Burlison JA, Zhang HG, Yan J and Guo H. 89Zr-Labeled anti-PD-L1 antibody fragment for evaluating in vivo PD-L1 levels in melanoma mouse model. Cancer Biother Radiopharm 2020; 35: 549-557.

[39] Massicano AVF, Song PN, Mansur A, White SL, Sorace AG and Lapi SE. [^{89}Zr]-Atezolizumab-PET imaging reveals longitudinal alterations in PDL1 during therapy in TNBC preclinical models. Cancers (Basel) 2023; 15: 2708.

[40] Verhoeff S, van de Donk PP, Aarntzen EHJG, Miedema IHC, Oosting S, Voortman J, Brouwers AH, Slingerland M, Heskamp S and Van Herpen CML. 89Zr-durvalumab PD-L1 PET in recurrent or metastatic (R/M) squamous cell carcinoma of the head and neck. J Clin Oncol 2020; 38: 3573-3573.

[41] Smit J, Borm FJ, Niemeijer AN, Huisman MC, Hoekstra OS, Boellaard R, Oprea-Lager DE, Vugts DJ, van Dongen GAMS, de Wit-van der Veen BJ, Thunnissen E, Smit EF and de Langen AJ. PD-L1 PET/CT imaging with radiolabeled durvalumab in patients with advanced-stage non-small cell lung cancer. J Nucl Med 2022; 63: 686-693.

[42] Verhoeff SR, van de Donk PP, Aarntzen EHJG, Oosting SF, Brouwers AH, Miedema IHC, Voortman J, Menke-van der Houven van Oordt WC, Boellaard R, Vriens D, Slingerland M, Hermsen R, Grunsven IVE, Heskamp S and van Herpen CML. (89)Zr-DFO-durvalumab PET/CT before durvalumab treatment in patients with recurrent or metastatic head and neck cancer. J Nucl Med 2022; 63: 1523-1530.

[43] Cheng Y, Shi D, Xu Z, Gao Z, Si Z, Zhao Y, Ye R, Fu Z, Fu W, Yang T, Xiu Y, Lin Q and Cheng D. 124I-labeled monoclonal antibody and fragment for the noninvasive evaluation of tumor PD-L1 expression in vivo. Mol Pharm 2022; 19: 3551-3562.

[44] Powles T, O'Donnell PH, Massard C, Arkenau HT, Friedlander TW, Hoimes CJ, Lee JL, Ong M, Sridhar SS, Vogelzang NJ, Fishman MN, Zhang J, Srinivas S, Parikh J, Antal J, Jin X, Gupta AK, Ben Y and Hahn NM. Efficacy and safety of durvalumab in locally advanced or metastatic urothelial carcinoma: updated results from a phase 1/2 open-label study. JAMA Oncol 2017; 3: e172411.

[45] Lee JM, Cimino-Mathews A, Peer CJ, Zimmer A, Lipkowitz S, Annunziata CM, Cao L, Harrell MI, Swisher EM, Houston N, Botesteanu DA, Taube JM, Thompson E, Ogurtsova A, Xu H, Nguyen J, Ho TW, Figg WD and Kohn EC. Safety and clinical activity of the programmed death-ligand 1 inhibitor durvalumab in combination with poly (ADP-Ribose) polymerase inhibitor olaparib or vascular endothelial growth factor receptor 1-3 inhibitor cediranib in women's cancers: a dose-escalation, phase I study. J Clin Oncol 2017; 35: 2193-2202.

[46] Hilton J, Cescon DW, Robinson A, Dhesy-Thind S, Taylor S, Awan A, Ng TL, Rushton M, Savard MF, Muyot L, Reeves MC, Hagerman L, Lui H, Bray M, Tu D, Seymour L and Gaudreau PO. Abstract P3-07-18: CCTG IND.239: a phase 2 study of combined CFI-400945 and durvalumab in patients with advanced triple negative breast cancer (aTNBC). Cancer Res 2023; 83: P3-07-18-P03-07-18.

[47] Ehlerding EB, Lee HJ, Barnhart TE, Jiang D, Kang L, McNeel DG, Engle JW and Cai W. Noninvasive imaging and quantification of radiotherapy-induced PD-L1 upregulation with 89Zr-Df-atezolizumab. Bioconjug Chem 2019; 30: 1434-1441.

[48] Li M, Ehlerding EB, Jiang D, Barnhart TE, Chen W, Cao T, Engle JW and Cai W. In vivo characterization of PD-L1 expression in breast cancer by immuno-PET with (89)Zr-labeled avelumab. Am J Transl Res 2020; 12: 1862-1872.

[49] Wissler HL, Ehlerding EB, Lyu Z, Zhao Y, Zhang S, Eshraghi A, Buuh ZY, McGuth JC, Guan Y, Engle JW, Bartlett SJ, Voelz VA, Cai W and Wang RE. Site-specific immuno-PET tracer to image PD-L1. Mol Pharm 2019; 16: 2028-2036.

[50] van de Watering FC, Rijpkema M, Perk L, Brinkmann U, Oyen WJ and Boerman OC. Zirconium-89 labeled antibodies: a new tool for molecular imaging in cancer patients. Biomed Res Int 2014; 2014: 203601.

[51] Anderson CJ and Ferdani R. Copper-64 radiopharmaceuticals for PET imaging of cancer: advances in preclinical and clinical research. Cancer Biother Radiopharm 2009; 24: 379-393.

[52] Mortimer JE, Bading JR, Colcher DM, Conti PS, Frankel PH, Carroll MI, Tong S, Poku E, Miles JK, Shively JE and Raubitschek AA. Functional imaging of human epidermal growth factor receptor 2-positive metastatic breast cancer using (64)Cu-DOTA-trastuzumab PET. J Nucl Med 2014; 55: 23-9.

[53] Stewart R, Morrow M, Hammond SA, Mulgrew K, Marcus D, Poon E, Watkins A, Mullins S, Chodorge M, Andrews J, Bannister D, Dick E, Crawford N, Parmentier J, Alimzhanov M, Babcook JS, Foltz IN, Buchanan A, Bedian V, Wilkinson RW and McCourt M. Identification and characterization of MEDI4736, an antagonistic anti-PD-L1 monoclonal antibody. Cancer Immunol Res 2015; 3: 1052-1062.

[54] Antonia SJ, Villegas A, Daniel D, Vicente D, Murakami S, Hui R, Yokoi T, Chiappori A, Lee KH, de Wit M, Cho BC, Bourhaba M, Quantin X, Tokito T, Mekhail T, Planchard D, Kim YC, Karapetis CS, Hiret S, Ostoros G, Kubota K, Gray JE, Paz-Ares L, de Castro Carpeño J, Wadsworth C, Melillo G, Jiang H, Huang Y, Dennis PA and Özgüroğlu M; PACIFIC Investigators. Durvalumab after chemoradiotherapy in stage III non-small-cell lung cancer. N Engl J Med 2017; 377: 1919-1929.

[55] Faiena I, Cummings AL, Crosetti AM, Pantuck AJ, Chamie K and Drakaki A. Durvalumab: an investigational anti-PD-L1 monoclonal antibody for the treatment of urothelial carcinoma. Drug Des Devel Ther 2018; 12: 209-215.

[56] Niemeijer AN, Leung D, Huisman MC, Bahce I, Hoekstra OS, van Dongen GAMS, Boellaard R, Du S, Hayes W, Smith R, Windhorst AD, Hendrikse NH, Poot A, Vugts DJ, Thunnissen E, Morin P, Lipovsek D, Donnelly DJ, Bonacorsi SJ, Velasquez LM, de Gruijl TD, Smit EF and de Langen AJ. Whole body PD-1 and PD-L1 positron emission tomography in patients with non-small-cell lung cancer. Nat Commun 2018; 9: 4664.

[57] Heskamp S, Hobo W, Molkenboer-Kuenen JD, Olive D, Oyen WJ, Dolstra H and Boerman OC. Noninvasive imaging of tumor PD-L1 expression using radiolabeled anti-PD-L1 antibodies. Cancer Res 2015; 75: 2928-2936.

[58] Zhang L, Zhang S, Wu J, Wang Y, Wu Y, Sun X, Wang X, Shen J, Xie L, Zhang Y, Zhang H, Hu K, Wang F, Wang R and Zhang MR. Linear peptide-based PET tracers for imaging PD-L1 in tumors. Mol Pharm 2023; 20: 4256-4267.

[59] Latgé A, Boisson F, Ouadi A, Averous G, Thomas L, Imperiale A and Brasse D. $^{64}CuCl_2$ PET imaging of 4T1-related allograft of triple-negative breast cancer in mice. Molecules 2022; 27: 4869.

[60] Zhang Y, Hong H, Engle JW, Bean J, Yang Y, Leigh BR, Barnhart TE and Cai W. Positron emission tomography imaging of CD105 expression with a 64Cu-Labeled monoclonal antibody: NOTA is superior to DOTA. PLoS One 2011; 6: e28005.

[61] Lv G, Sun X, Qiu L, Sun Y, Li K, Liu Q, Zhao Q, Qin S and Lin J. PET imaging of tumor PD-L1 expression with a highly specific nonblocking single-domain antibody. J Nucl Med 2020; 61: 117-122.

[62] Zhou H, Bao G, Wang Z, Zhang B, Li D, Chen L, Deng X, Yu B, Zhao J and Zhu X. PET imaging of an optimized anti-PD-L1 probe 68Ga-NODAGA-BMS986192 in immunocompetent mice and non-human primates. EJNMMI Res 2022; 12: 35.

[63] Bouleau A, Nozach H, Dubois S, Kereselidze D, Chevaleyre C, Wang CI, Evans MJ, Lebon V, Maillère B and Truillet C. Optimizing immuno-PET imaging of tumor PD-L1 expression: pharmacokinetic, biodistribution, and dosimetric comparisons of ^{89}Zr-labeled anti-PD-L1 antibody formats. J Nucl Med 2022; 63: 1259-1265.

[64] Houghton JL, Abdel-Atti D, Scholz WW and Lewis JS. Preloading with unlabeled CA19.9 targeted human monoclonal antibody leads to improved PET imaging with 89Zr-5B1. Mol Pharm 2017; 14: 908-915.

[65] Hegi-Johnson F, Rudd S, Hicks RJ, De Ruysscher D, Trapani JA, John T, Donnelly P, Blyth B, Hanna G, Everitt S, Roselt P and MacManus MP. Imaging immunity in patients with cancer using positron emission tomography. NPJ Precis Oncol 2022; 6: 24.

[66] Wahl RL, Sgouros G, Iravani A, Jacene H, Pryma D, Saboury B, Capala J and Graves SA. Normal-tissue tolerance to radiopharmaceutical therapies, the knowns and the unknowns. J Nucl Med 2021; 62 Suppl 3: 23S-35S.

[67] Ehlerding EB, England CG, Jiang D, Graves SA, Kang L, Lacognata S, Barnhart TE and Cai W. CD38 as a PET imaging target in lung cancer. Mol Pharm 2017; 14: 2400-2406.